Journal of
Synchrotron
Radiation

ISSN 0909-0495

Received 14 November 2007
Accepted 27 June 2008

Visualization of age-dependent myocardial metabolic impairment in cardiomyopathic model hamster obtained by fluorescent X-ray computed tomography using I-127 BMIPP

Thet-Thet-Lwin,[a] Tohoru Takeda,[a]* Jin Wu,[a] Qingkai Huo,[b] Tetsuya Yuasa,[b] Kazuyuki Hyodo[c] and Takao Akatsuka[b]

[a]Graduate School of Comprehensive Human Sciences, University of Tsukuba, Japan, [b]Graduate School of Engineering, Yamagata University, Japan, and [c]High Energy Accelerator Research Organization, Japan. E-mail: ttakeda@md.tsukuba.ac.jp

Fluorescent X-ray computed tomography (FXCT) enables visualization of myocardial fatty acid metabolism by using non-radio-iodinated I-5-(*p*-iodophenyl)-3-(*R*,*S*)-methylpentadecanoice acid (BMIPP). In this experiment, age-dependent myocardial metabolic impairment was successfully imaged and analyzed quantitatively in J2N-k cardiomyopathic hamster using FXCT.

Keywords: fluorescent X-ray computed tomography; age-dependent metabolic impairment; cardiomyopathy; myocardial fatty acid; BMIPP.

1. Introduction

Using various radionuclide chemical agents, micro-imaging techniques such as micro-positron emission tomography (PET) and micro-single-photon emission computed tomography (SPECT) play an important role in basic biomedical research to assess the functional impairment of small animals using various heart disease models.

Fluorescent X-ray methods are used as highly sensitive imaging techniques to detect very low contents of non-radioactive media and/or heavy-atomic-number elements. Thus, we originally designed a fluorescent X-ray computed-tomography (FXCT) imaging system that did not require the preparation of specimens like in planar mode (Takeda, Akiba *et al.*, 1996), and the sensitivity of the FXCT was about 80-fold higher than that of absorption X-ray computed tomography (CT) (Yu *et al.*, 2001). The cross-sectional distribution of iodine in human thyroid was imaged first (Rust & Weigelt, 1998; Takeda *et al.*, 2000, 2001), and our interests are now towards the use of FXCT in determining tracer elements including iodine. Since radio-iodinated I-5-(*p*-iodophenyl)-3-(*R*,*S*)-methylpentadecanoic acid (^{123}I-BMIPP) is a potential tracer for detecting the myocardial fatty acid metabolism in clinical SPECT studies (Fujibayashi *et al.*, 1990; Inoue *et al.*, 2007; Ogata, 1989; Thet-Thet-Lwin *et al.*, 2003), we chose to use this agent for FXCT imaging. We successfully imaged the state of the impaired myocardial fatty acid metabolism in a 22-week-old J2N-k cardiomyopathic model hamster using our FXCT system with non-radio-iodinated BMIPP (^{127}I-BMIPP) (Thet-Thet-Lwin *et al.*, 2007).

The J2N-k cardiomyopathic hamster, obtained by cross-breeding a Bio14.6 cardiomyopathic Syrian hamster and a Golden hamster, is a standard model of cardiomyopathy. J2N-k hamsters begin to show slight fibrosis at eight weeks old, exhibit moderate cardiac dysfunction, degeneration of cardiomyocyte and interstitial fibrosis at about 20 weeks, and finally die owing to congestive heart failure when approximately one year old (Saito *et al.*, 1998; Nagano & Saito, 1998). Recently, these biological data, exhibiting a variety of metabolic abnormalities, have provided us with important information for understanding human cardiac disease and for finding keys for earlier diagnosis and therapy for human cardiomyopathy. By extending the achievement of our previous result, here the age-dependent myocardial fatty acid metabolic impairment was imaged and analyzed quantitatively in J2N-k cardiomyopathic hamsters by FXCT using ^{127}I-BMIPP.

2. Materials and methods

2.1. Objects and preparation

Eight-week, 12-week, 15-week, 20-week and 25-week J2N-k cardiomyopathic hamsters and age-matched J2N-n normal hamsters were examined. ^{127}I-BMIPP (0.08 mg g^{-1} weight) was injected through the femoral vein of each hamster under anesthesia. Each heart labelled with BMIPP was extracted after 5 min of injection and fixed by formalin. Experiments were undertaken in accordance with the Medical Committee for the Use of Animals in Research of the University of Tsukuba, and conformed to the guidelines of the American Physiological Society.

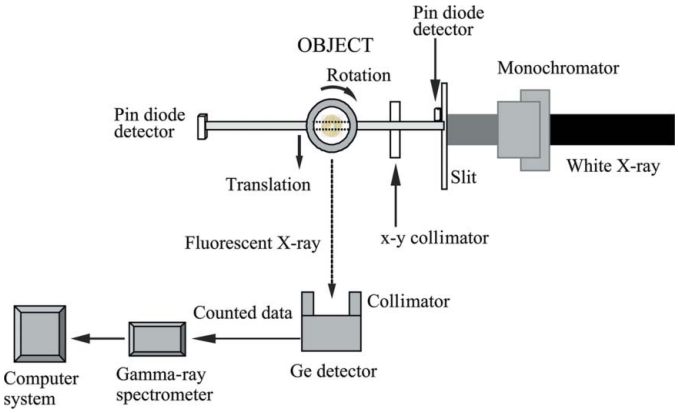

Figure 1
Schematic diagram of the fluorescent X-ray CT system.

2.2. FXCT

FXCT was carried out using a silicon (220) double-crystal monochromator to select the X-ray energy, an X-ray slit system, a scanning table for the subject, a highly purified Ge detector with a parallel collimator, two pin-diode detectors and a computer system (Fig. 1) (Thet-Thet-Lwin *et al.*, 2007).

The monochromatic X-ray energy was set to 37 keV to separate the peak energy of the fluorescent iodine $K\alpha$ line from Compton scatter (Takeda, Maeda *et al.*, 1996). The photon flux in front of the object was approximately 10^8 photons mm^{-2} s^{-1}, and the X-ray absorption dose was 2.7 Gy. The incident monochromatic X-ray beam was collimated into a pencil beam with square cross section (0.25 mm $\times$ 0.5 mm) using the X-ray slit system. Fluorescent X-rays were detected by the HPGe detector in photon-counting mode. Furthermore, to reduce the amount of Compton radiation captured by the same detector, the HPGe detector was positioned perpendicular to the incident monochromatic X-ray beam. Experiments were carried out at the synchrotron X-ray source at the Photon Factory, High Energy Accelerator Research Organization, Tsukuba, Japan.

2.3. FXCT data acquisition parameter and reconstruction

The formalin-fixed heart labelled with BMIPP was imaged by FXCT when placed in an acrylic object cell. Here, two short-axis slices at mid-ventricular level of a cardiomyopathic hamster heart (1 mm interval) and one short-axis slice from a normal hamster were imaged.

The projection data were acquired at each sampling point from 0.25 mm translational steps over the sample diameter and 3° rotational steps over 180°. The data acquisition time for each sampling point was 7 s. By observing the spectrum of the iodine fluorescent $K\alpha$ line at each CT scanning step, the distribution of iodine in the object was imaged. FXCT images were reconstructed using the algebraic reconstruction technique including the attenuation process of the incident beam and the emitted fluorescent X-ray within the object (Yuasa *et al.*, 1997).

2.4. Quantitative image analysis

For quantitative analysis of FXCT images, the left-ventricle image was divided into four regions, *i.e.* the anterior wall, lateral wall, inferior wall and septum, interactively. The fluorescent X-ray intensity of iodine was measured in each region of the normal and cardiomyopathic myocardium. The myocardial BMIPP uptake was estimated by referring to the linear regression curve between the fluorescent X-ray intensity and iodine concentration using a basic phantom study, as described previously (Thet-Thet-Lwin *et al.*, 2007). For each region the relative uptake of BMIPP was defined as the ratio of regional intensity to maximal intensity in the four regions.

2.5. Quantitative image analysis

The results are expressed as the mean $\pm$ standard deviation (SD) and are analyzed by unpaired *t*-test. A value of probability $p < 0.01$ was considered statistically significant.

3. Results

Typical FXCT images are shown in Fig. 2. In normal hamsters of all ages and cardiomyopathic hamsters of age eight weeks the BMIPP was distributed almost homogeneously. However, in the cardiomyopathic hamsters at age 12 weeks the BMIPP uptake decreased slightly and was distributed heterogeneously. In the cardiomyopathic hamsters aged more than 12 weeks the distribution of BMIPP became progressively more heterogeneous. At 25 weeks the BMIPP uptake decreased significantly in the septum and inferior wall. The distribution of the BMIPP uptake was not significantly different between two slices in the same cardiomyopathic hamster.

The relationship between the myocardial area and BMIPP uptake for normal and cardiomyopathic hamsters is shown in Fig. 2(*b*). The myocardial BMIPP uptake in the cardiomyopathic hamsters shifted to a lower value compared with that of the normal hamsters. To assess the myocardial area with reduced fatty acid metabolism for each age of the cardiomyopathic hamsters, a lower limit of the normal BMIPP uptake value was set as the mean BMIPP uptake value minus 2SD for the normal hamsters.

The percentage of the myocardial area with reduced fatty acid metabolism was 7.5%, 17.1%, 24.3% and 47.4% of the whole of the left myocardium for eight-, 12-, 15- and 25-week cardiomyopathic hamsters, respectively. The mean BMIPP uptake in age-matched normal and cardiomyopathic hamsters was 178.2 $\pm$ 19.2 μg ml^{-1} *versus* 171.4 $\pm$ 20.7 μg ml^{-1}, 178.6 $\pm$ 19.1 μg ml^{-1} *versus* 163.7 $\pm$ 23.5 μg ml^{-1}, 176.3 $\pm$ 20.8 μg ml^{-1} *versus* 155.9 $\pm$ 26.3 μg ml^{-1}, and 180.1 $\pm$ 20.1 μg ml^{-1} *versus* 143.3 $\pm$ 29.1 μg ml^{-1} for ages of eight weeks, 12 weeks, 15 weeks and 25 weeks, respectively (Fig. 2*c*). The mean BMIPP uptake values of the cardiomyopathic myocardium were significantly decreased at 15 and 25 weeks ($p < 0.05$).

The relative regional BMIPP uptake for all ages of normal and cardiomyopathic hamsters is given in Table 1. In the

Table 1
Relative regional uptake of BMIPP in normal and cardiomyopathic hamsters.

Objects are one normal hamster per age group (n = 1) and two hamsters (n = 2) for cardiomyopathy. n.s. = not statistically significant.

	Regions				
Group	Anterior wall	Lateral wall	Inferior wall	Septum	p value
Control (8–25 weeks: n = 1)	0.95 ± 0.04	0.92 ± 0.05	0.95 ± 0.05	0.98 ± 0.02	n.s.
Cardiomyopathy (8 weeks: n = 2)	0.93 ± 0.08	0.91 ± 0.08	0.92 ± 0.09	0.94 ± 0.05	n.s.
Cardiomyopathy (12 weeks: n = 2)	0.96 ± 0.05	0.87 ± 0.09	0.87 ± 0.08	0.94 ± 0.10	n.s.
Cardiomyopathy (15 weeks: n = 2)	0.97 ± 0.07	0.94 ± 0.08	0.73 ± 0.05†	0.83 ± 0.07†	<0.01
Cardiomyopathy (25 weeks: n = 2)	0.96 ± 0.07	0.93 ± 0.06	0.71 ± 0.06†	0.77 ± 0.08†	<0.01

† Statistically significant; lower value in inferior wall and septum.

normal hamsters and cardiomyopathic hamsters aged less than 12 weeks the relative uptake of BMIPP was not significantly different in any region. However, in the cardiomyopathic hamsters the relative BMIPP uptake decreased significantly in the septum and inferior wall for those hamsters more than 15 weeks old (Table 1).

The morphological structures such as papillary muscle, wall thickness and left-ventricular diameter were revealed clearly by FXCT, as shown in Fig. 2(*a*). In cardiomyopathy an increased left-ventricular diameter and decreased wall thickness were observed from 15 weeks, and the significant left-ventricular dilatation and wall thinning occurred at 25 weeks.

4. Discussion

The FXCT revealed almost homogeneous myocardial BMIPP accumulation in normal hamsters aged from eight to 25 weeks and in cardiomyopathic hamsters aged eight weeks. However, BMIPP accumulated heterogeneously and its uptake decreased in cardiomyopathic hamsters aged more than 12 weeks; in particular, the degree of decreased BMIPP uptake was prominent in the inferior wall and septum. The regional heterogeneity of BMIPP accumulation was observed significantly in the older cardiomyopathic hamsters. Abnormal

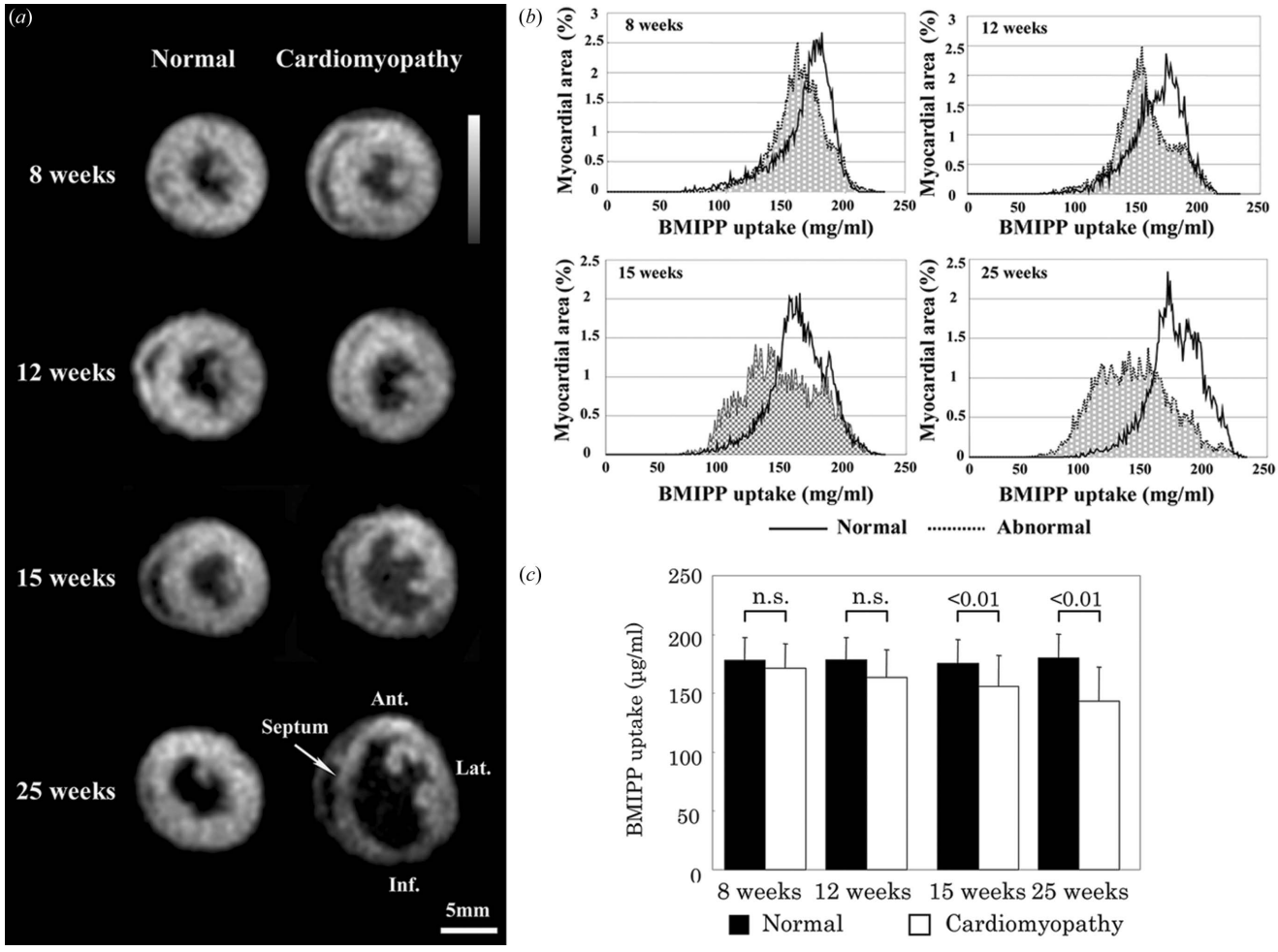

Figure 2
(*a*) FXCT images of mid-ventricular slices, and (*b*) the distribution of myocardial BMIPP uptake corresponding to the slices in (*a*). (*c*) The average BMIPP uptake for each case in (*a*). Ant: anterior wall; Lat: lateral wall; Inf: inferior wall.

accumulation of BMIPP depicted by FXCT was more severe than expected from histological changes, and the BMIPP uptake was also decreased in the inferior wall and septum at 20 weeks for the J2N-k cardiomyopathgic hamster (Thet-Thet-Lwin *et al.*, 2003, 2007). In addition, the area of reduced BMIPP uptake increased progressively depending on age. The area with reduced BMIPP uptake (47.4% at the mid-left ventricle) at 25 weeks was 6.3 times broader than that at eight weeks. This phenomenon is considered to be due to myocardial metabolic impairment in the cardiomyopathic hearts because similar pathological changes in fatty acid metabolism were also reported in previous studies using radio-iodinated BMIPP (Mochizuki *et al.*, 1997; Thet-Thet-Lwin *et al.*, 2003, 2004).

In addition, morphological changes such as left-ventricular dilatation and decreased wall thickness were observed in the late phase of cardiomyopathy, and these changes had occurred more severely and more prominently in the older cardiomyopathic hamsters.

Thus, FXCT could clearly depict the transition of the age-dependent fatty acid metabolism, and was able to assess the quantitative analysis for cardiomyopathy. As an alternative technique to the conventional autoradiogram with radioactive agents, FXCT has the advantage of not using any radioactive agent. For researchers and pharmacologists the use of a non-radioactive agent allows easy preparation and observation of samples using various pathological staining techniques, and effective development of new drugs without considering and protecting against radiation exposure.

On our prototype FXCT system (Takeda *et al.*, 2004; Takeda, 2005), long data acquisition times are required, *i.e.* seven hours per slice to image with 0.25 mm spatial resolution. Therefore we are now introducing a new mechanical scanning technique to reduce the scan points outside the object, and a revised detector system to obtain FXCT data much faster. With an improved FXCT system, CT data are expected to be acquired about 28 times faster than with the present prototype system by shortening the distance between the detector and the object from 80 mm to 15 mm. This allows the data acquisition time to be shortened to 15 min, and exposure to be reduced to less than 100 mGy.

Since FXCT can image the object using the CT configuration, this technique can also be used in *in vivo* observation. At present, *in vivo* imaging techniques, such as micro-SPECT or micro-PET, of small animals are under development; however, for both techniques the use of radionuclide agents is indispensable, and their spatial resolutions are limited to $\sim$1 mm and 1–0.5 mm, respectively. The FXCT system provides an *in vitro* imaging with 0.25 mm spatial resolution, so this technique might be used for high-spatial-resolution *in vivo* imaging without radionuclide agent. Therefore, FXCT might be used as a molecular imaging technique to analyze the various myocardial conditions in small animals considered as human disease models.

We thank N. Sunaguchi MS, Mr S. Nasukawa and Mr K. Kobayashi for their experimental help, Ms Y. Kawata for preparation of the manuscript, Ms S. Reffold for advice on English expressions, and Nihon Medi-Physics, Japan, for supplying the BMIPP. This research was partially supported by Grant-In-Aid for Scientific Researches (Nos. 19390313 and 17390326) and for Special Coordination Funds from the Ministry of Education, Culture, Sports, Science and Technology, and was performed under the auspices of the High Energy Accelerator Research Organization (2005G308, 2007G643).

References

Fujibayashi, Y., Yonekura, Y., Takemura, Y., Wada, K., Matsumoto, K. & Tamaki, N. (1990). *J. Nucl. Med.* **31**, 1818–1822.
Inoue, A., Fukimoto, S., Yamashina, S. & Yamazaki, J. (2007). *Ann. Nucl. Med.* **21**, 399–404.
Mochizuki, T., Tsukamoto, E., Ono, T., Itoh, K., Kanegae, K., Katoh, C., Shiga, T., Nakada, K., Kohya, T. & Tamaki, N. (1997). *Ann. Nucl. Med.* **4**, 299–306.
Nagano, M. & Saito, N. (1998). *Zoku Shinzou Taisya Jikkenhou*, pp. 191–196.
Ogata, M. (1989). *KAKUIGAKU*, **26**, 69–76.
Rust, G. F. & Weigelt, J. (1998). *IEEE Trans. Nucl. Sci.* **45**, 75–88.
Saito, N., Iwai, T., Fujii, M., Kato, M. & Nagano, M. (1998). *Shinkin no Kohzoh to Taisha*, **21**, 125–133.
Takeda, T. (2005). *Nucl. Instrum. Methods Phys. Res. A*, **548**, 38–46.
Takeda, T., Akiba, M., Yuasa, T., Kazama, M., Hoshino, A., Watanabe, Y., Hyodo, K., Dilmanian, F. A., Akatsuka, T. & Itai, Y. (1996). *Proc. SPIE*, **2708**, 685–695.
Takeda, T., Maeda, T., Yuasa, T., Ito, T., Sakamoto, K., Wu, J., Hyodo, K., Dilmaninan, F. A., Akatsuka, T. & Itai, Y. (1996). *Med. Imag. Tech.* **14**, 183–194.
Takeda, T., Momose, A., Yu, Q., Yuasa, T., Dilmanian, F. A., Akatsuka, T. & Itai, Y. (2000). *Cell. Mol. Biol.* **46**, 1077–1088.
Takeda, T., Tsuchiya, Y., Kuroe, T., Zeniya, T., Wu, J., Thet-Thet-Lwin, Yashiro, T., Yuasa, T., Hyodo, K., Matsumura, K., Dilmania, F. A., Itai, Y. & Akatsuka, T. (2004). *AIP Proc.* **705**, 1320–1323.
Takeda, T., Yu, Q., Yashiro, T., Zeniya, T., Wu, J., Hasegawa, Y., Thet-Thet-Lwin, Hyodo, K., Yuasa, T., Dilmanian, F. A., Akatsuka, T. & Itai, Y. (2001). *Nucl. Instrum. Methods Phys. Res. A*, **467–468**, 1318–1321.
Thet-Thet-Lwin, Takeda, T., Wu, J., Fumikura, Y., Iida, K., Kawano, S., Yamaguchi, I. & Itai, Y. (2003). *Eur. J. Nucl. Med. Mol. Imaging*, **30**, 966–973.
Thet-Thet-Lwin, Takeda, T., Wu, J., Sunaguchi, N., Murakami, T., Mouri, S., Nasukawa, S., Huo, Q., Yuasa, T., Hyodo, K. & Akatsuka, T. (2007). *J. Synchrotron Rad.* **14**, 158–162.
Thet-Thet-Lwin, Takeda, T., Wu, J., Tsuchiya, Y. & Itai, Y. (2004). *Ann. Nucl. Med.* **18**, 195–202.
Yu, Q., Takeda, T., Yuasa, T., Hasegawa, Y., Wu, J., Thet-Thet-Lwin, Hyodo, K., Dilmanian, F. A., Itai, Y. & Aktsuka, T. (2001). *J. Synchrotron Rad.* **8**, 1030–1034.
Yuasa, T., Akiba, M., Takeda, T., Kazama, M., Hoshino, Y., Watanabe, Y., Hyodo, K., Dilmanian, F. A., Akatsuka, T. & Itai, Y. (1997). *IEEE Trans. Nucl. Sci.* **44**, 54–62.